Research Article | Vol. 27, No. 5 | 4 Mar 2019 | OPTICS EXPRESS 7064
Optics EXPRESS

Residual amplitude modulation and its mitigation in wedged electro-optic modulator

ZHIXIU LI,[1,2] YUHANG TIAN,[1,2] YAJUN WANG,[1,2] WEIGUANG MA,[2,3] AND YAOHUI ZHENG[1,2,*]

[1]*The State Key Laboratory of Quantum Optics and Quantum Optics Devices, Institute of Opto-Electronics, Shanxi University, Taiyuan 030006, China*
[2]*Collaborative Innovation Center of Extreme Optics, Shanxi University, Taiyuan 030006, China*
[3]*The State Key Laboratory of Quantum Optics and Quantum Optics Devices, Institute of Laser Spectroscopy, Shanxi University, Taiyuan 030006, China*
[*]*yhzheng@sxu.edu.cn*

Abstract: We theoretically analyze and experimentally investigate the dependence of residual amplitude modulation (RAM) on the beam radius within the electro-optic crystal (EOC), the wedge angle of the EOC and the overlap efficiency between the extraordinary and ordinary beams, and the overlap efficiency is determined by the distance from the wedge facet to the downstream polarizer. The results show that the RAM with the maximum optical path difference Δ at the edge of light spot presents a sinc-like curve, and the magnitude of Δ is directly proportional to the beam radius and the wedge angle. As a scaling factor, with the decrease of the overlap efficiency between the ordinary and extraordinary beams, the RAM can be further reduced.

© 2019 Optical Society of America under the terms of the OSA Open Access Publishing Agreement

1. Introduction

Squeezed states are an important nonclassical light field, since their first observation, they have been applied to a diversity of fields, for example, generating the Schrödinger cat states for quantum information networks [1,2] and improving the sensitivity for gravitational wave detector [3,4]. For all these applications, a strong and stable squeezing factor is beneficial. The standard technique to generate squeezed state is to use a sub-threshold optical parametric oscillator (OPO) [5–9]. In order to obtain the high-level and stable squeezed light, the optical cavities and relative phases must be locked accurately and steadily by using the Pound-Drever-Hall (PDH) locking technique in the squeezed states generation experiments [10–13].

For a PDH locking system, an electro-optic modulator (EOM) is an essential component, and employed to provide the phase modulation of the incident light beam and generate the error signal for the cavity and phase locking [14]. Unfortunately, there produce inevitably the unwanted residual amplitude modulation (RAM) during the process of optical phase modulation [15–21]. The RAM causes an imbalance in sidebands, which induces the lineshape distortion and the zero baseline drift of PDH error signal [12, 22]. Therefore, it degrades the cavity- and phase-locking performances and is especially detrimental in the quantum noise stability of the squeezed state [12, 13, 23].

Early and follow-up investigations have revealed that the RAM arises primarily from the birefringence of the electro-optic crystal (EOC) [15, 22]. Under ideal conditions, the polarization direction of the laser beam parallels to the principal axis of the EOC, and there is a pure phase modulation. In practice, it is inevitable to have a small polarization noise of the laser beam, and axis mismatch between the incident polarized and the principal axis of the EOC. Consequently, the laser beam presents two mutually orthogonal components (the ordinary and extraordinary beams) in the EOC. For the conventional EOM, the EOC have two parallel end facets, the output of the modulated light after the EOM includes two orthogonal sets of carriers and two sidebands, which are superposed in space. The phase difference between the ordinary and extraordinary

#356799 https://doi.org/10.1364/OE.27.007064
Journal © 2019 Received 4 Jan 2019; revised 14 Feb 2019; accepted 15 Feb 2019; published 25 Feb 2019

Optics EXPRESS

beams is uniform in the whole light spot, and fluctuates with the temperature and stress variations [24, 25]. Polarizing optical components downstream will make the intensity fluctuate consistently within the spot with the phase delay difference generating the RAM. Compounding matters, the phase delay of the two beams is sensitive to the temperature and stress variations, which makes the RAM drift with time. Numerous efforts have been made to suppress the RAM, e.g., active feedback control of EOM [15, 26-31], usage of proton-exchanged EOM [32], Brewster-cutting EOM [33], wedged EOM [23, 34].

The basic principle of reducing the RAM by the wedged EOM is that the deflection angles of the ordinary and extraordinary beams are different through the wedged facet due to the natural birefringence of the crystal. The ordinary beam after propagating a certain distance d is thoroughly separated from the extraordinary beam in space, the polarization interference between the two beams is eliminated. The RAM originating from the birefringence effect and the etalon effect of EOC is significantly reduced. The distance d is concerned with the wedge angle and the beam radius. At less than the distance d, the two beams are overlapped in space. In general, we think that the RAM of the wedged EOM dependent of the overlap efficiency between the two beams is reduced at the expense of enlarging the system size [35]. The contradiction becomes more complicated for the squeezed state generation system because that it includes more than one PDH locking loops.

Further investigation finds that the RAM of the wedged EOM is not only dependent on the distance d, but other mechanisms. For the wedged EOM, the difference of the phase delay varies with the position of the wedge facet. As a result, the output beam from the wedged EOM usually contains various polarization states. Polarizing optical components downstream will make the light spot show the interference pattern that moves with the temperature and stress variations. The intensity variation with the fringe movement generally presents a declining trend as the number of interference fringes in the light spot is increased. Maybe if a specific condition is met, the total intensity keeps constant and is independent on the fringe movement. Therefore, the topic, which is the particular focus of this paper, is the investigation and mitigation countermeasure of RAM of the wedged EOM.

In this paper, we theoretically analyze and experimentally investigate the dependence of RAM on the beam radius within the EOC, the wedge angle of the EOC and the beam overlap efficiency determined by the distance from the wedge facet to the downstream polarizer. The researches show that the RAM with the maximum optical path difference Δ at the edge of the light spot presents a sinc-like function. The Δ value is determined by the beam radius within the EOC and the wedge angle of the EOC. The dependence of RAM on the overlap efficiency between the extraordinary and ordinary beams is studied provided that the Δ value is fixed. The experimental results are in good agreement with the theoretical analysis, which is of great significance in the development of compact squeezed and entanglement sources.

2. RAM model for wedged electro-optical modulator

Figure 1 shows the generation principle of RAM originating from the birefringence of the EOC. The z- and y-axes are the principal axes of the extraordinary and ordinary waves, respectively. The laser propagates along the x-axis, two end faces are perpendicular to the x-axis for the conventional design. An EOM is constructed by combining the EOC with an electric field parallel to the z-axis. An inevitable axis mismatch between the incident polarized and principal axes of the EOC make the laser beam divided into the ordinary and extraordinary beams in the EOC. The phase difference between the extraordinary and ordinary beams after the EOC can be expressed as:

$$\Delta\phi_{parallel} = \frac{2\pi}{\lambda}\left(n_e - n_o\right) l = \frac{2\pi}{\lambda}\left(\mu_e - \mu_o\right)\delta T l, \tag{1}$$

Optics EXPRESS

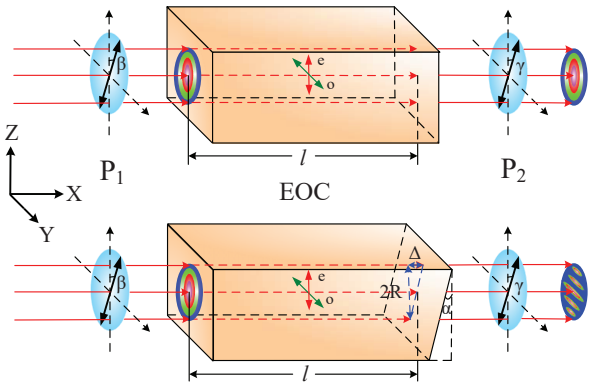

Fig. 1. Generation principle of RAM originating from the birefringence of the EOC. EOC: electro-optic crystal; P: polarizer.

where λ is the laser wavelength; l is the length of the crystal; n_e and n_o are the refractive indices of the extraordinary and ordinary beams, respectively; μ_e and μ_o are the temperature coefficients of refractive indices n_e and n_o, respectively, the differential temperature coefficients $\mu_e - \mu_o$ is $3.956\times10^{-5}\ ^oC^{-1}$ at temperature 20–30 ^oC [25]. For the parallel EOC, the crystal length l is a constant, and the phase difference is equal everywhere in the whole light spot. Polarizing optical components downstream will make the orthogonal polarization beams interfere mutually. The variation of the phase difference originating from the difference of the thermos-optical coefficient results in the laser intensity fluctuation as a whole.

Distinguishing from the parallel EOC, the crystal length l is not a constant for the wedged EOC, which depends on the position of the beam in the wedge facet. The phase difference after the wedged EOC can be expressed as [36]:

$$\Delta\phi_{wedged} = \frac{2\pi}{\lambda}\left(\mu_e - \mu_o\right)\delta T\left(l + \frac{1}{2}z\Delta\right), \tag{2}$$

where Δ is the maximum optical path difference at the edge of the light spot, which is dependent on the beam radius R within the EOC, and the wedge angle α of the EOC, it can be expressed as $\Delta = 2R\tan\alpha$, and for the parallel EOC, $\alpha = 0°$; z (-1≤ z ≤ 1) is the normalized coordinate parameter. The crystal length of the EOC is l at z=0 that corresponds to the center of the beam. At the edge of the beam, the coordinate parameter z is ±1.

With the intensity distribution function of Gaussian beam, the RAM for the wedged EOM is concerned with the intensity integral in the light spot, which can be expressed as:

$$V_{RAM} = C\eta \iint\limits_{y^2+z^2=1} \exp\left[-2\left(y^2+z^2\right)\right]\sin\left[\frac{2\pi}{\lambda}\left(\mu_e - \mu_o\right)\delta T\left(l + \frac{1}{2}z\Delta\right)\right]dydz, \tag{3}$$

where C=2abKA^{2}J$_1$ (M) B [12, 15, 22], A is the amplitude of the incident light; a=sinβ sin γ and b=cosβ cos γ are the alignment factors, the polarizers before and after the EOM have polarization angles of β and γ with respect to the z-axis of the crystal; J$_1$ (M) is the first order Bessel function, M is the modulation index; K is the joint gain of the photodetection and the demodulation process; B is the normalized factor. In the later experiment, the above experiment parameters remain unchanged, the theoretical analysis is demonstrated by simply changing the beam radius R and wedge angle α. η is the overlap efficiency between the extraordinary and ordinary beams, which decreases with the increasing distance d from the wedge facet to polarizing optical components downstream in a certain wedge angle. The parallel EOM corresponds to the case $\Delta = 0$.

Optics EXPRESS

According to Eq. (3), we can obtain the normalized RAM with the change of the maximum optical path difference Δ. While not considering the influence of the overlap efficiency, the RAM with the maximum optical path difference Δ at the edge of the light spot is shown in Fig. 2. In the case of the parallel EOM, the Δ value is zero, the RAM is a constant, which is normalized to 1 for the sake of the convenient comparison. In the case of the wedged EOM, the RAM with Δ presents a sinc-like function that is damped oscillation. If a specific condition is met, the RAM is zero, independent of the temperature and stress variations. The first zero-point of the RAM appears at the Δ value of approximately 24 μm, when the laser wavelength is 1064 nm. The RAM has some separate zero-points with the increasing of the Δ value. Limited by the measurement accuracy of the beam radius R and wedge angle α in an actual experiment, it is impossible to meet exactly the zero-point of the RAM. However, the overall trend ensures that the RAM can obviously decrease with a large Δ comparing with the parallel EOM even if we miss the zero-point. In the case of $\Delta = 92\mu m$, the maximum RAM of the wedged EOM is only 0.5% of that of the parallel EOM, as can be seen at point Q in the inset of Fig. 2, and supposed the overlap efficiency is 100%. The cross section of the EOC defines the upper limit of the beam radius R. At a certain R, a large wedge angle α can help to reduce the RAM. However, the larger wedge angle α is, the larger deflection angle of the output beam is, the large deflection angle increases the difficulty of beam alignment. Thus, there has an optimal value of the wedge angle α at which the RAM is small enough, not at the expense of increasing significantly the difficulty of beam alignment.

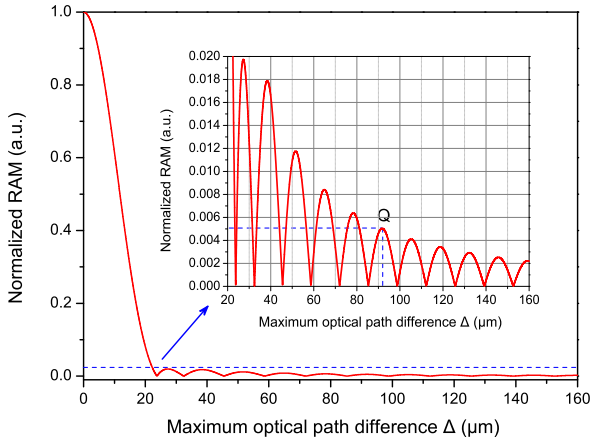

Fig. 2. RAM of the wedged EOM as a function of the maximum optical path difference Δ.

The overlap efficiency η is another factor of affecting the RAM, as a scaling factor. For the parallel EOM, the overlap efficiency η does always equal to 100%, independent of the beam radius R and the distance d. In the case of the wedged EOM, it benefits from the difference of the refraction angles at the wedge facet, the overlap efficiency η decreases with the distance d increasing. Thus, by optimizing these parameters, including the beam radius R, the wedge angle α, and the distance d from the wedge facet to the downstream polarizer, the RAM can be further reduced but not at the cost of enlarging the system size.

3. Experimental results and analysis

Figure 3 shows the experimental setup for measuring the RAM with the changes of the beam radius R within the EOC, the wedge angle α of the EOC and the distance d from the wedge facet to the polarizing optical components downstream. A homemade single-frequency Nd:YVO_4 laser

Optics EXPRESS

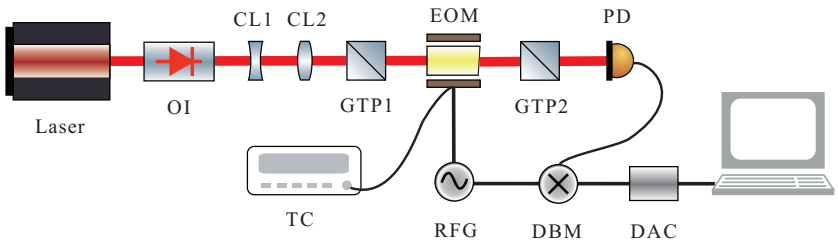

Fig. 3. Experimental setup for measuring the RAM. EOM: electro-optical modulator; OI: optical isolator; GTP: Glan–Thompson polarizer; CL: concave lens or convex lens; TC: temperature controller; PD: photodetector; RFG: radio-frequency generator; DBM: doubly balanced mixer; DAC: data acquisition card.

at 1064 nm is used as the light source [37]. An optical isolator (OI) in front of the laser is used to minimize the backreflections. The linearly polarized beam incident in the EOM is ensured with a purity of better than 1:100000 by using a Glan–Thompson prism (GTP). Another GTP is located after the EOM as a downstream polarizing optical component, which aligns along the propagation direction of the extraordinary wave. The EOC is made up of a natural birefringence Lithium niobate ($LiNbO_3$) crystal with MgO-doped concentration of 5%, with the dimension of $3{\times}4 \times 40$ mm^3. The beam radius R within the EOC can be flexibly adjusted by the concave lens (CL1) and convex lens (CL2). It is worthy of note that the beam waist should be located at the center of the EOC as much as possible in order to ensure that there has the constant beam radius along the crystal axis. The EOC temperature is controlled by a heating plate posted in the EOM, the heating plate is driven by a temperature controller (TC). The GTP2 output is directly fed into an radio-frequency (RF) photodetector (PD) to read the modulation signal which corresponds to the situation far from the cavity resonance. A RF signal with 10 MHz is split into two parts: one is used to drive the EOM, the other is mixed with the PD output to generate the PDH error signal, that is, the zero baseline of the error signal. The mixer output is fed into a NI data acquisition card (DAC) to record the zero baseline drift of the error signal, which is an indicator of the RAM.

Limited by the cross-section of the EOC, there has a maximum waist radius of 1000 μm in the experiment, producing the transmission efficiency of 99%. The dependence of the RAM on the beam radius R is quantified with four different EOMs, which have the identical configurations except for the wedge angle α. The wedge angle α of the four samples is 0°, 0.5°, 1.5°, and 4°, respectively. The two GTPs are deliberately rotated by approximately 4° away from their optimized polarization angles in order to achieve an enough amplitude of the RAM, which can help reduce the measurement error. To isolate the measurement from the temperature effect, at each measurement cycle the temperature of the EOC is scanned to search for a maximum RAM. In a full measurement cycle, no experimental parameters other than the wedge angle α and beam radius R are varied. The RAM is measured by simply replacing the EOM with various wedge angles at each beam radius R. Then we repeat the above measurement at the beam waist from 100 μm to 1000 μm with the step of 100 μm. The measurement schedule ensures that the measurement error is as small as possible.

Figure 4 shows the measurement results about the normalized RAM. The discrete points are the results of experimental values, and the curves are the fitting results according to Eq. (3). When the wedge angle $\alpha = 0°$, corresponding to the parallel EOM, the RAM is constant independent of the beam radius R. In the case of $\alpha \neq 0°$, the RAM decreases with the beam radius R increasing at a certain α. As the wedge angle α is increased, the dependence of the RAM on the beam radius R becomes acute. With the wedge angle α of 0.5°, the maximum Δ is 17 μm when the beam radius R is 1000 μm, the optimal RAM is 18% of that of parallel EOM, as can be seen in Fig. 2. With the wedge angle α of 1.5°, the sinc-like curve shows four

Optics EXPRESS

peaks at the maximum Δ, the remaining RAM is about 1%. However, it reduces the flexibility of choice of the beam radius R. In the case of R=1000 μm, the Δ value is approximately 140 μm at the wedge angle α of 4°. The corresponding RAM is only 0.25% of that of parallel EOM, which is small enough to the application of squeezed state generation. At this point, the deflection angle originating from the wedge angle is about 5°, the deviation is easily compensated in downstream experiment. The experimental results are in good agreement with the theoretical analysis. The results provide theoretically a new mechanism of analyzing the RAM of the wedge EOM, and verify experimentally its correctness, which is of great significance in the development of compact squeezed and entanglement sources.

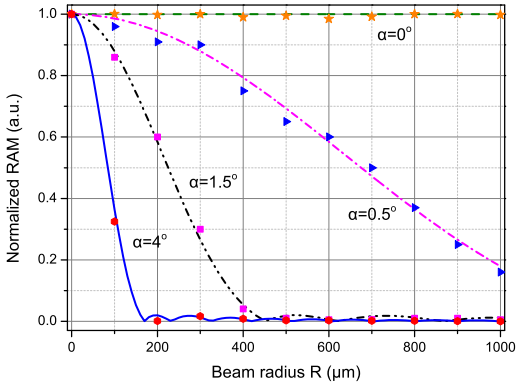

Fig. 4. Dependence of the RAM on the beam radius R at the wedge angle α of 0°, 0.5°, 1.5°, 4°.

All the data in Fig. 4 is measured at the GTP2 close to the output end of the EOM where the overlap efficiency η between the extraordinary and ordinary beams can be considered as 100%. In order to investigate the dependence of RAM on the overlap efficiency η in Eq. (3), the RAM is quantified with the distance d, with the beam radius R and the wedge angle α of 500 μm and 0.5°, respectively. All the data is taken under the condition that no experimental parameters other than the distance d from the wedge facet to the GTP2 is varied. The results are shown in Fig. 5, which is normalized according to the measurement results in Fig. 4. These data verifies of the theoretical analysis in Eq. (3). As the distance d is increased, the overlap efficiency η as a scaling factor decreases, which can further reduce the RAM comparing with that of the GTP2 close to the output end of the EOM. Last but not least, the RAM is only dependent on the distance d from the wedge facet to the GTP2, and independent on the distance d from the wedge facet to the PD.

4. Conclusion

In conclusion, we have presented a new mechanism of analyzing the RAM of the wedged EOM. Since the difference of the phase delay varies with the position of the wedge facet, the output beam from the wedged EOM shows no Gaussian distribution, but the interference pattern owing to the polarizing optical components downstream. The interference fringe moves with temperature and stress variations. The intensity variation with the fringe movement generally presents on a declining trend as the number of the interference fringes in the light spot increased. According to the theoretical analysis and experimental investigation in this paper, the degree of RAM shows a sinc-like function versus the maximum optical path difference Δ at the edge of the light spot. The Δ is direct proportional to the beam radius R within the EOC and the wedge angle α of the EOC. Therefore, the RAM can be effectively reduced by enlarging the beam radius R and the wedge angle α. If a specific condition is met, the RAM is zero, independent of the temperature

and stress variations. As a scaling factor, with the decrease of the overlap efficiency between the ordinary and extraordinary beams, the RAM can be further reduced. The experimental results are in good agreement with the theoretical analysis, which is of great significance in the development of compact squeezed and entanglement sources.

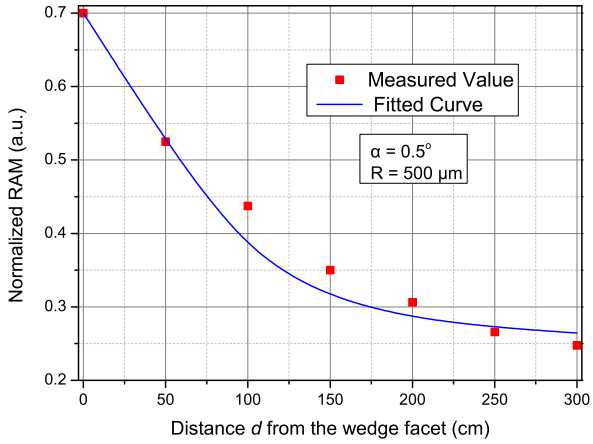

Fig. 5. Dependence of RAM on the distance d from the wedge facet.

Funding

National Natural Science Foundation of China (NSFC) (Grant No.11654002, 61575114, 11804207, 11874250); National Key Research and Development Program of China (2016YFA0301401); Program for Sanjin Scholar of Shanxi Province; Program for Outstanding Innovative Teams of Higher Learning Institutions of Shanxi; Fund for Shanxi "1331 Project" Key Subjects Construction.

References

1. A. Ourjoumtsev, R. Tualle-Brouri, J. Laurat, and P. Grangier, "Generating optical Schrödinger Kittens for quantum information processing," Science **312**, 83–86 (2006).
2. J. S. Neergaard-Nielsen, B. Melholt Nielsen, C. Hettich, K. Mølmer, and E. S. Polzik, "Generation of a superposition of odd photon number states for quantum information networks," Phys. Rev. Lett. **97**, 083604 (2006).
3. K. Goda, O. Miyakawa, E. E. Mikhailov, S. Saraf, R. Adhikari, K. McKenzie, R. Ward, S. Vass, A. J. Weinstein, and N. Mavalvala, "A quantum-enhanced prototype gravitational-wave detector," Nat. Phys. **4**, 472–476 (2008).
4. The LIGO Scientific Collaboration, "A gravitational wave observatory operating beyond the quantum shot-noise limit," Nat. Phys. **7**, 962–965 (2011).
5. L. A. Wu, H. J. Kimble, J. L. Hall, and H. F. Wu, "Generation of squeezed states by parametric down conversion," Phys. Rev. Lett. **57**, 2520-2523 (1986).
6. T. Eberle, S. Steinlechner, J. Bauchrowitz, V. Handchen, H. Vahlbruch, M. Mehmet, H. Muller-Ebhardt, and R. Schnabel, "Quantum enhancement of the zero-area sagnac interferometer topology for gravitational wave detection," Phys. Rev. Lett. **104**, 251102 (2010).
7. M. Mehmet, S. Ast, T. Eberle, S. Steinlechner, H. Vahlbruch, and R, Schnabel, "Squeezed light at 1550 nm with a quantum noise reduction of 12.3 dB," Opt. Express **19**, 25763-25772 (2011).
8. H. Vahlbruch, M. Mehmet, K. Danzmann, and R. Schnabel, "Detection of 15 dB squeezed states of light and their application for the absolute calibration of photoelectric quantum efficiency," Phys. Rev. Lett. **117**, 110801 (2016).
9. T. Serikawa, J. Yoshikawa, K. Makino, and A. Frusawa, "Creation and measurement of broadband squeezed vacuum from a ring optical parametric oscillator," Opt. Express **24**, 28383-28391 (2016).
10. E. Oelker, G. Mansell, M. Tse, J. Miller, F. Matichard, L. Barsotti, P. Fritschel, D. E. McClelland, M. Evans, and N. Mavalvala, "Ultra-low phase noise squeezed vacuum source for gravitational wave detectors," Optica **3**, 682–685 (2016).
11. S. Dwyer, L. Barsotti, S. S. Y. Chua, M. Evans, M. Factourovich, D. Gustafson, T. Isogai, K. Kawabe, A. Khalaidovski, P. K. Lam, M. Landry, N. Mavalvala, D. E. McClelland, G. D. Meadors, C. M. Mow-Lowry, R. Schnabel, R. M.

Optics EXPRESS

S. Schofield, N. Smith-Lefebvre, M. Stefszky, C. Vorvick, and D. Sigg, "Squeezed quadrature fluctuations in a gravitational wave detector using squeezed light," Opt. Lett. **21**, 19047–19060 (2013).
12. Z. X. Li, X. C. Sun, Y. J. Wang, Y. H. Zheng, and K. C. Peng, "Investigation of residual amplitude modulation in squeezed state generation system," Opt. Express **26**, 18957–18968 (2018).
13. W. H. Yang, S. P. Shi, Y. J. Wang, W. G. Ma, Y. H. Zheng, and K. C. Peng, "Detection of stably bright squeezed light with the quantum noise reduction of 12.6 dB by mutually compensating the phase fluctuations," Opt. Lett. **42**, 4553–4556 (2017).
14. E. D. Black, "An introduction to Pound–Drever–Hall laser frequency stabilization," Am. J. Phys. **69**, 79-87 (2001).
15. N. C. Wong, and J. L. Hall, "Servo control of amplitude modulation in frequency-modulation spectroscopy: demonstration of shot-noise-limited detection," J. Opt. Soc. Am. B, **2**, 1527–1533 (1985).
16. J. Sathian and E. Jaatinen,"Intensity dependent residual amplitude modulation in electro-opticc phase modulators," Appl. Opt. **51**, 3684–3691 (2012).
17. J. Sathian and E. Jaatinen, "Reducing residual amplitude modulation in electro-optic phase modulators by erasing photorefractive scatter," Opt. Express **21**, 12309–12317 (2013).
18. P. Ehlers, I. Silander, J. Y. Wang, and O. Axner, "Fiber-laser-based noise-immune cavity-enhanced optical heterodyne molecular spectrometry instrumentation for Doppler-broadened detection in the 10^{-12} cm^{-1} $Hz^{-1/2}$ region," J. Opt. Soc. Am. B **29**, 1305–1315 (2012).
19. K. Kokeyama, K. Izumi, W. Korth, N. Smith-Lffebvre, K. Arai, and R. Adhikari, "Residual amplitude modualtion in interferomatric gravitational wave detectors," J. Opt. Soc. Am. A **31**, 81–88 (2014).
20. I. Silander, P. Ehlers, J. Y. Wang, and O. Axner, "Frequency modulation background signals from fiber-based electro optic modulators are caused by crosstalk," J. Opt. Soc. Am. B **29**, 916-923 (2012).
21. E. A. Whittaker, M. Gehrtz, and G. C. Bjorklund, "Residual amplitude modulation in laser electro-optic phase modulation," J. Opt. Soc. Am. B **2**, 1320–1326 (1985).
22. H. Shen, L. F. Li, J. Bi, J. Wang, and L. S. Chen, "Systematic and quantitative analysis of residual amplitude modulation in Pound-Drever-Hall frequency stabilization," Phys. Rev. A **92**, 063809 (2015).
23. Z. X. Li, W. G. Ma, W. H. Yang, Y. J. Wang, and Y. H. Zheng, "Reduction of zero baseline drift of the Pound–Drever–Hall error signal with a wedged electro-optical crystal for squeezed state generation," Opt. Lett. **41**, 3331–3334 (2016).
24. Z. X. Li, L. H. Zhao, W. Tan, W. G. Ma, G. Zhao, X. F. Fu, L. Dong, L. Zhang, W. B. Yin, and S. T. Jia, "Investigation and cancellation of residual amplitude modulation in fiber electro-optic modulator based frequency modulation gas sensing technique," Sens. Actuators B **196**, 23–30 (2014).
25. L. F. Li, F. Liu, C. Wang, and L. S. Chen, "Measurement and control of residual amplitude modulation in optical phase modulation," Rev. Sci. Instrum. **83**, 043111 (2012).
26. W. G. Ma, Z. X. Li, W. Tan, G. Zhao, X. F. Fu, L. Zhang, L. Dong, W. B. Yin, and S. T. Jia, "Servo control of high degree of linear polarization output from polarization-maintaining fiber and its applicaiton in fiber-component based frequency modulation spectroscopy," Appl. Phys. Express **6**, 112501 (2013).
27. F. Du Burck, O. Lopez, and A. El Basri, "Narrow-band correction of the residual amplitude modulation in frequency-modulation spectroscopy," IEEE Trans. Instrum. Meas.**52**, 288–291 (2003).
28. W. Zhang, M. J. Martin, C. Benko, J. L. Hall, J. Ye, C. Hagemann, T. Legero, U. Sterr, F. Riehle, G. D. Cole, and M. Aspelmeyer, "Reduction of residual amplitude modulation to 1×10^{-6} for frequency modulation and laser stabilization," Opt. Lett. **39**, 1980–1983 (2014).
29. L. F. Li, H. Shen, J. Bi, C.Wang, S. S. Lv, and L. S. Chen, "Analysis of frequency noise in ultra-stable optical oscillators with active control of residual amplitude modulation," Appl.Phys. B **117**,1025 (2014).
30. H. Müller, S. Herrmann, T. Schuldt, M. Scholz, E. Kovalchuk, and A. Peters, "Offset compensation by use of amplitude-modulated sidebands in optical frequency standards," Opt. Lett. **28**, 2186–2188 (2003).
31. T. Kessler, C. Hagemann, C. Grebing, T. Legero, U. Sterr, F. Riehle, M. J. Martin, L. Chen, and J. Ye, "A sub-40-mHz-linewidth laser based on a silicon single-crystal optical cavity," Nat. Photonics **6**, 687–692 (2012).
32. A. Foltynowicz, I. Silander, and O. Axner, "Reduction of background signals in fiber-based NICE-OHMS," J. Opt. Soc. Am. B **28**, 2797-2805 (2011).
33. Z. Y. Tai, L. L. Yan, Y. Y. Zhang, X. F. Zhang, W. G. Guo, S. G. Zhang, and H. F. Jiang, "Electro-optic modulator with ultra-low residual amplitude modulation for frequency modulation and laser stabilization," Opt. Lett. **41**, 5584–5587 (2016).
34. K. L. Dooley, M. A. Arain, D. Feldbaum, V. V. Frolov, M. Heintze, D. Hoak, E. A. Khazanov, A. Lucianetti, R. M. Martin, G. Mueller, O. Palashov, V. Quetschke, D. H. Reitze, R. L. Savage, D. B. Tanner, L. F. Williams, and W. Wu, "Thermal effects in the input optics of the enhanced laser interferometer gravitational-wave observatory interferometers," Rev. Sci. Instrum. **83**, 033109 (2012).
35. V. M. Quetschke, W. Wu, L. Williams, M. A. Arain, R. Martin, D. Reitze, D. B. Tanner, and G. Mueller, "Method and apparatus for modulating light," US Patent 0164302 (July 7, 2011).
36. J. H. Ge, Z. Chen, Y. F. Chen, C. Y. Chen, Y. F. Zhai, J. Zhang, Z. Sui, H. H. Lin, J. J. Wang, and Q. H. Deng, "Optimized design of parameters for wedge-crystal depolarizer," Mech. Aerosp. Eng. **110–116**, 3351–3357 (2012).
37. H. D. Lu, J. Su, Y. H. Zheng, and K. C. Peng, "Physical conditions of single-longitudinal-mode operation for high-power all-solid-state lasers," Opt. Lett. **39**, 1117-1120 (2014).